

1
2
3
4 ***Technical note:***

5 **Analyses of Uncertainties and Scaling**

6 **of Groundwater Level Fluctuations**

7

8 Xiuyu Liang^{a,b} , You-Kuan Zhang^{a*,b,c}

9 ^aCenter for Hydrosciences Research, Nanjing University,
10 Nanjing, Jiangsu 210093, P.R. China

11 ^bSchool of Earth Sciences and Engineering, Nanjing University,
12 Nanjing, Jiangsu 210093, P.R. China

13 ^cDepartment of Geoscience, University of Iowa,
14 Iowa City, Iowa 52242, USA

15 *Corresponding author

16 Phone: +86 25-83594485, Fax: +86 25-83596670,
17 Email: ykzhang@nju.edu.cn

18

19

20

21 Resubmitted to *Hydrology and Earth System Sciences*
22 May, 2015

23 **Abstract**

24 Analytical solutions for the variance, covariance, and spectrum of groundwater level,

25 $h(x, t)$, in an unconfined aquifer described by a linearized Boussinesq equation with

26 random source/sink and initial and boundary conditions were derived. It was found

27 that in a typical aquifer the error in $h(x, t)$ in early time is mainly caused by the

28 random initial condition and the error reduces as time progresses to reach a constant

29 error in later time. The duration during which the effect of the random initial

30 condition is significant may last a few hundred days in most aquifers. The constant

31 error in $h(x, t)$ in later time is due to the combined effects of the uncertainties in the

32 source/sink and flux boundary: the closer to the flux boundary, the larger the error.

33 The error caused by the uncertain head boundary is limited in a narrow zone near the

34 boundary and remains more or less constant over time. The aquifer system behaves

35 as a low-pass filter which filters out high-frequency noises and keeps low-frequency

36 variations. Temporal scaling of groundwater level fluctuations exists in most part of

37 a low permeable aquifer whose horizontal length is much larger than its thickness

38 caused by the temporal fluctuations of areal source/sink.

39 **Key words:** Uncertainty of groundwater levels; Temporal scaling; Random source/sink;

40 Random initial and boundary conditions.

41 **1. Introduction**

42 Groundwater level or hydraulic head (h) is the main driving force for water flow
43 and advective contaminant transport in aquifers and thus the most important variable
44 studied in groundwater hydrology and its applications. Knowledge about h is critical
45 in dealing with groundwater-related environmental problems, such as over-pumping,
46 subsidence, sea water intrusion, and contamination. One often found that the data
47 about groundwater level is limited or unavailable in a hydrogeological investigation.

48 In such cases the groundwater level distribution and its temporal variation are
49 usually obtained with an analytical or numerical solution to a groundwater flow
50 model.

51 It is obvious that errors always exit in the groundwater levels calculated or
52 simulated with analytical or numerical solutions. The main sources of errors include
53 the simplification or approximation in a conceptual model and the uncertainties in
54 the model parameters. Problems in conceptualization or model structure were dealt
55 with by many researchers (Neuman, 2003;Rojas et al., 2010;Ye et al., 2008;Rojas et
56 al., 2008;Refsgaard et al., 2007;Zeng et al., 2013). The uncertainties in the model
57 parameters (e.g., hydraulic conductivity, recharge rate, evapotranspiration, and river
58 conductance) were investigated based on generalized likelihood uncertainty
59 estimation and Bayesian methods (Nowak et al., 2010;Neuman et al., 2012;Rojas et
60 al., 2008;Rojas et al., 2010). The uncertainty in groundwater level has been one of
61 the main research topics in stochastic subsurface hydrology for more than three
62 decades. Most of these studies were focused on the spatial variability of groundwater

63 level due to aquifers' heterogeneity (Dagan, 1989;Gelhar, 1993;Zhang, 2002). Little
64 attention has been given to the uncertainties in groundwater level due to temporal
65 variations of hydrological processes, e.g., recharge, evapotranspiration, discharge to
66 a river, and river stage (Bloomfield and Little, 2010;Zhang and Schilling,
67 2004;Schilling and Zhang, 2012;Liang and Zhang, 2013a;Zhu et al., 2012).

68 Uncertainties of groundwater level fluctuations have been studied by Zhang and
69 Li (2005, 2006) and most recently by Liang and Zhang (2013a). Based on a linear
70 reservoir model with a white noise or temporally-correlated recharge process, Zhang
71 and Li (2005, 2006) derived the variance and covariance of $h(t)$ by considering only
72 a random source or sink process assuming deterministic initial and boundary
73 conditions. Liang and Zhang (2013a) extended the studies of Zhang and Li (2005,
74 2006) and carried out non-stationary spectral analysis and Monte Carlo simulations
75 using a linearized Boussinesq equation, and investigated the temporospatial
76 variations of groundwater level. However, the only random process considered by
77 Liang and Zhang (2013a) is the source/sink. Temporal scaling of groundwater levels
78 discovered first by Zhang and Schilling Zhang and Schilling (2004) was verified in
79 several studies (Zhang and Li, 2005, 2006; Bloomfield and Little, 2010; Zhang and
80 Yang, 2010; Zhu et al., 2012; Schilling and Zhang, 2012). However, we do not know
81 the effect of random boundary conditions on temporal scaling of groundwater levels.

82 In this study we extended above-mentioned work by considering the
83 groundwater flow in a bounded aquifer described by a linearized Boussinesq
84 equation with a random source/sink as well as random initial and boundary

85 conditions since the latter processes are known with uncertainties. The objectives of
 86 this study are 1) to derive analytical solutions for the covariance, variance and
 87 spectrum of groundwater level, and 2) to investigate the individual and combined
 88 effects of these random processes on uncertainties and scaling of $h(x, t)$. In the
 89 following we will first present the formulation and analytical solutions, then discuss
 90 the results, and finally draw some conclusions.

91

92 **2. Formulation and Solutions**

93 Under the Dupuit assumption, the one-dimensional transient groundwater flow in
 94 an unconfined aquifer near a river (Fig. 1) can be approximated with the linearized
 95 Boussinesq equation (Bear, 1972) with the initial and boundary conditions, i.e.,

$$96 \quad T \frac{\partial^2 h}{\partial x^2} + W(t) = S_y \frac{\partial h}{\partial t} \quad (1a)$$

$$97 \quad h(x, t)|_{t=0} = H_0(x); \quad T \frac{\partial h}{\partial x} \Big|_{x=0} = Q(t); \quad h(x, t)|_{x=L} = H(t) \quad (1b)$$

98 where T [L/T] is the transmissivity, h [L] is the hydraulic head or groundwater level
 99 above the bottom of the aquifer which is assumed to be horizontal, $W(t)$ [L/T] is the
 100 time-dependent source/sink term representing areal recharge or evapotranspiration, S_y
 101 is the specific yield, $H_0(x)$ [L] is the initial condition, $Q(t)$ [L^2/T] is the
 102 time-dependent flux at the left boundary, $H(t)$ [L] is the time-dependent water level at
 103 the right boundary, L [L] is distance from the left to the right boundary, x [L] is the
 104 coordinate, and t [T] is time. In this study the initial head $H_0(x)$ is taken to be a
 105 spatially random variable, and the source/sink, $W(t)$, the flux to the left boundary, $Q(t)$,
 106 and the head at the right boundary, $H(t)$, are all taken to be temporally random

107 processes and spatially deterministic. The parameters T and S_Y are taken to be
 108 constant.

109 The groundwater level, $h(x, t)$, the three random processes, $W(t)$, $Q(t)$, and $H(t)$,
 110 and the random variable, $H_0(x)$, are expressed in terms of their respective ensemble
 111 means plus small perturbations,

$$112 \quad h(x, t) = \langle h(x, t) \rangle + h'(x, t) \quad (2a)$$

$$113 \quad W(t) = \langle W(t) \rangle + W'(t); \quad Q(t) = \langle Q(t) \rangle + Q'(t) \quad (2b)$$

$$114 \quad H(t) = \langle H(t) \rangle + H'(t); \quad H_0(x) = \langle H_0(x) \rangle + H_0'(x) \quad (2c)$$

115 where $\langle \rangle$ stands for ensemble average and $'$ for perturbation. The initial condition
 116 $H_0(x)$ in (1) can be any function. For the conceptualization of the groundwater flow
 117 presented in Fig. 1, the steady-state condition can be reached in this aquifer after a
 118 rainfall or during a wet season. Thus the steady-state solution to this model were often
 119 adopted as initial condition in previous research (Liang and Zhang, 2012, 2013a, b).

120 Thus, in this study, we set initial condition $H_0(x)$ to be the steady-state solution to
 121 the one-dimensional groundwater flow equation, i.e., $H_0(x) = h_0 + 0.5W_0(L^2 - x^2)/T$,
 122 where h_0 [L] is the constant groundwater level at the right boundary and W_0 [L/T] is
 123 the spatially constant recharge rate (Liang and Zhang, 2012). Since h_0 is taken to be
 124 constant, the source of the uncertainty in the initial head $H_0(x)$ is due to random W_0
 125 only. Thus, the mean and perturbation of $H_0(x)$ can be written as,

$$126 \quad \langle H_0(x) \rangle = h_0 + 0.5\langle W_0 \rangle(L^2 - x^2)/T \quad \text{and} \quad H_0'(x) = 0.5W_0'(L^2 - x^2)/T, \quad \text{respectively.}$$

127 By substituting Eq. (2), $\langle H_0(x) \rangle$, and $H_0'(x)$ into Eq. (1) and taking expectation, one
 128 obtains the mean flow equation with the mean initial and boundary conditions as

$$129 \quad T \frac{\partial^2 \langle h \rangle}{\partial x^2} + \langle W \rangle = S_Y \frac{\partial \langle h \rangle}{\partial t} \quad (3a)$$

130
$$\langle h(x,0) \rangle = h_0 + \frac{\langle W_0 \rangle}{2T} (L^2 - x^2); \quad T \frac{\partial \langle h \rangle}{\partial x} \Big|_{x=0} = \langle Q \rangle; \quad \langle h(L,t) \rangle = \langle H(t) \rangle \quad (3b)$$

131 Subtracting Eq. (3) from (1) leads to the following perturbation equation with the
132 initial and boundary conditions

133
$$T \frac{\partial^2 h'}{\partial x^2} + W' = S_Y \frac{\partial h'}{\partial t} \quad (4a)$$

134
$$h'(x,0) = \frac{W_0'}{2T} (L^2 - x^2); \quad T \frac{\partial h'}{\partial x} \Big|_{x=0} = Q'; \quad h'(L,t) = H'(t) \quad (4b)$$

135 The analytical solution to Eq. (4) can be derived with integral-transform methods
136 (Ozisik, 1968) given by

137
$$h' = \frac{2}{L} \sum_{n=0}^{\infty} e^{-\beta b_n^2 t} \cos(b_n x) \left[\frac{(-1)^n}{b_n^3 T} W_0' + \beta \int_0^t e^{\beta b_n^2 \xi} \left[\frac{(-1)^n}{T b_n} W'(\xi) - \frac{Q'(\xi)}{T} + H'(\xi) (-1)^n b_n \right] d\xi \right] \quad (5)$$

138 where $\beta = T / S_Y$, $b_n = (2n+1)\pi / (2L)$. Using Eq. (5), the temporal covariance of the
139 groundwater level fluctuations can be derived as

140
$$C_{hh}(x, t_1; x, t_2) = E[h'(x, t_1)h'(x, t_2)] = \frac{4}{L^2} \sum_{m=0}^{\infty} \sum_{n=0}^{\infty} e^{-\beta(b_m^2 t_1 + b_n^2 t_2)} \cos(b_m x) \cos(b_n x) \left[\frac{(-1)^{m+n}}{T^2 b_m^3 b_n^3} \sigma_{W_0}^2 + \beta^2 \int_0^{t_1} \int_0^{t_2} e^{\beta(b_m^2 \xi + b_n^2 \rho)} \left[\frac{(-1)^{n+m}}{T^2 b_m b_n} C_{WW}(\xi, \rho) + \frac{C_{QQ}(\xi, \rho)}{T^2} + C_{HH}(\xi, \rho) (-1)^{m+n} b_m b_n \right] d\xi d\rho \right] \quad (6)$$

141 in which $\sigma_{W_0}^2$ is the variance of W_0 , and $C_{WW}(\xi, \rho)$, $C_{QQ}(\xi, \rho)$ and $C_{HH}(\xi, \rho)$ are the
142 temporal auto-covariance of $W(t)$, of $Q(t)$, and $H(t)$, respectively. We assume that
143 $W(t)$, $Q(t)$, and $H(t)$ are uncorrelated in order to simplify our analyses. It is shown in
144 Eq. (6) that the head covariance depends on the variance of W_0 and the covariances
145 of $W(t)$, $Q(t)$, and $H(t)$ and this equation can be evaluated for any random $W(t)$, $Q(t)$,
146 and $H(t)$. We assume that these processes are white noises as employed in previous

147 studies (Gelhar, 1993; Hantush and Marino, 1994; Liang and Zhang, 2013a). More
 148 realistic randomness of these processes will be considered in future studies.

149 Following *Gelhar* (1993, p.34), we express the spectra of $W(t)$, $Q(t)$, and $H(t)$ as

150 $S_{WW} = \sigma_W^2 \lambda_W / \pi$, $S_{QQ} = \sigma_Q^2 \lambda_Q / \pi$, and $S_{HH} = \sigma_H^2 \lambda_H / \pi$, respectively, where σ_W^2 ,

151 σ_Q^2 , and σ_H^2 are the variances and λ_W , λ_Q , and λ_H are the correlation time

152 intervals of these three processes, respectively. The corresponding covariance of

153 $W(t)$, $Q(t)$ and $H(t)$ are $C_{WW}(\xi, \rho) = 2\sigma_W^2 \lambda_W \delta(\xi - \rho)$, $C_{QQ}(\xi, \rho) = 2\sigma_Q^2 \lambda_Q \delta(\xi - \rho)$,

154 and $C_{HH}(\xi, \rho) = 2\sigma_H^2 \lambda_H \delta(\xi - \rho)$. Substituting these covariance into (6) and taking

155 integration, one obtain analytical solution of head covariance

$$156 C_{hh}(x', t', \tau') = \frac{4\beta L^2}{T^2} \sum_{m=0}^{\infty} \sum_{n=0}^{\infty} \cos(b'_m x') \cos(b'_n x') \left\{ e^{-\left[\left(b'^2_m + b'^2_n\right)t' + \left(b'^2_n - b'^2_m\right)\frac{\tau'}{2}\right]} \frac{L^2 (-1)^{m+n} \sigma_{W_0}^2}{\beta b'^3_m b'^3_n} \right. \\ \left. + 2 \frac{\left(e^{-b'^2_m \tau'} - e^{-2b'^2_m t'}\right)}{\left(b'^2_m + b'^2_n\right)} \left[\frac{(-1)^{m+n} \sigma_W^2 \lambda_W}{L^2} + \frac{\sigma_Q^2 \lambda_Q}{L^2} + \frac{(-1)^{m+n} b'_m b'_n T^2 \sigma_H^2 \lambda_H}{L^4} \right] \right\} \quad (7)$$

157 where $\tau' = t'_2 - t'_1$ and $t' = (t'_2 + t'_1)/2$. The analytical solution for the head variance can
 158 be obtain by setting $\tau' = 0$

$$159 \sigma_h^2(x', t') = \frac{4\beta L^2}{T^2} \sum_{m=0}^{\infty} \sum_{n=0}^{\infty} \cos(b'_m x') \cos(b'_n x') \left\{ e^{-\left(b'^2_m + b'^2_n\right)t'} \frac{L^2}{\beta} \frac{(-1)^{m+n} \sigma_{W_0}^2}{b'^3_m b'^3_n} + \right. \\ \left. 2 \frac{1 - e^{-2b'^2_m t'}}{\left(b'^2_m + b'^2_n\right)} \left[\frac{(-1)^{m+n} \sigma_W^2 \lambda_W}{b'_m b'_n} + \frac{\sigma_Q^2 \lambda_Q}{L^2} + \frac{(-1)^{m+n} b'_m b'_n T^2 \sigma_H^2 \lambda_H}{L^4} \right] \right\} \quad (8)$$

160 where

$$161 t' = \frac{t}{t_c}; \quad x' = \frac{x}{L}; \quad t_c = \frac{L^2}{\beta}; \quad b'_n = \frac{(2n+1)\pi}{2}$$

162 in which $t_c (= S_Y L^2 / (KM)) [1/T]$ is a characteristic timescale (Gelhar, 1993) where
 163 the transmissivity (T) is replaced by the product of the hydraulic conductivity (K) and
 164 the average saturated thickness (M) of the aquifer. The characteristic timescale (t_c) is

165 an important parameter and its value for most shallow aquifers is usually larger than
 166 100 day since the horizontal extent of a shallow aquifer is usually much larger than its
 167 thickness. For instance, the value of t_c is 250 days for a sandy aquifer with $L=100\text{m}$,
 168 $M=10\text{m}$, $K=1\text{m/day}$, and $S_y=0.25$.

169 The spectral density of $h(x, t)$ can't be derived by ordinary Fourier transform
 170 since the head covariance and variance depend on time t' and thus $h(x, t)$ are
 171 temporally non-stationary as shown in Eqs. (7) and (8). Priestley (1981) defined the
 172 spectral density of non-stationary processes (Wigner spectrum) as the Fourier
 173 transform of time-dependent auto-covariance with fixed reference time t and derived
 174 time-dependent spectral density. In order to obtain the spectrum of $h(x, t)$, we applied
 175 Priestley's method and obtained the time-dependent spectral density (Priestley, 1981;
 176 Zhang and Li, 2005; Liang and Zhang, 2013a), i.e.,

$$177 \begin{aligned} S_{hh}(x, t, \omega) &= \frac{1}{2\pi} \int_{-\infty}^{\infty} C_{hh}(x, t, \tau) e^{-i\omega\tau} d\tau \\ &= \sum_{m=0}^{\infty} \sum_{n=0}^{\infty} \cos(b_m x) \cos(b_n x) \frac{2t_c(b_n^2 - b_m^2)}{\beta^2(b_n^2 - b_m^2)^2 / 4 + \omega^2} \frac{(-1)^{m+n} \sigma_{W_0}^2}{\pi T^2 b_m^3 b_n^3} + \\ &\quad \sum_{m=0}^{\infty} \sum_{n=0}^{\infty} \cos(b_m x) \cos(b_n x) \frac{8\beta b_m^2}{t_c(b_m^2 + b_n^2)} \frac{1}{\beta^2 b_m^4 + \omega^2} \left[\frac{(-1)^{m+n} S_{WW}}{T^2 b_m b_n} + \frac{S_{QQ}}{T^2} + (-1)^{m+n} b_m b_n S_{HH} \right] \end{aligned} \quad (9)$$

178 where ω is angular frequency and $\omega = 2\pi f$, f is frequency, and $i = \sqrt{-1}$. It is seen in
 179 Eq. (9) that the spectrum S_{hh} is dependent on not only frequency and locations but
 180 also time t . The time-dependent term (i.e., first term) in Eq. (9) is caused by the
 181 random initial condition and is proportional to $e^{-\beta(b_m^2 + b_n^2)t}$ which decays quickly with
 182 t . We evaluated the first term in the Eq. (9) by setting $t=0$ and found that it is much
 183 smaller than the second term in Eq. (9). We thus ignored the first term and evaluated
 184 the spectrum using the approximation,

185
$$S_{hh}(x', \omega) = \sum_{m=0}^{\infty} \sum_{n=0}^{\infty} \frac{8\beta b_m^2 \cos(b_m' x') \cos(b_n' x')}{t_c (b_m'^2 + b_n'^2) (\beta^2 b_m'^4 / L^4 + \omega^2)} \left[\frac{(-1)^{m+n} S_{ww} L^2}{T^2 b_m' b_n'} + \frac{S_{qq}}{T^2} + \frac{(-1)^{m+n} b_m' b_n' S_{hh}}{L^2} \right] \quad (10)$$

186

187 **3. Results and Discussion**

188 **3.1 Variance of groundwater levels**

189 The general expression of the head variance in Eq. (8) depends on the variances
 190 of the four random processes, $\sigma_{W_0}^2$, σ_w^2 , σ_q^2 , and σ_h^2 . In the following we will study
 191 their individual and combined effects on the head variation and focus our attention
 192 only on the variance of $h(x, t)$. The dimensionless standard deviation of $h(x, t)$, σ'_h ,
 193 or the square root of the dimensionless variance ($\sigma_h'^2$) as a function of the
 194 dimensionless time (t') were evaluated and presented in the left column of Fig. 2 at
 195 fixed dimensionless locations (x'). The σ'_h as a function of x' was evaluated and
 196 presented in the right column of Fig. 2 at fixed t' .

197 We first evaluate the effect of the random initial condition due to the random
 198 term, W_0 , by setting $\sigma_w^2 = \sigma_q^2 = \sigma_h^2 = 0$. In this case the dimensionless variance in Eq.
 199 (8) reduces to

200
$$\sigma_h'^2(x', t') = \sum_{m=0}^{\infty} \sum_{n=0}^{\infty} \frac{(-1)^{m+n}}{b_m'^3 b_n'^3} \cos(b_m' x') \cos(b_n' x') e^{-(b_m'^2 + b_n'^2)t'} \quad (11)$$

201 where $\sigma_h'^2 = \sigma_h^2 T^2 / (4L^4 \sigma_{W_0}^2)$. The changes of the σ'_h with x' and t' were
 202 presented in Fig 2a and 2b, respectively. It is shown in Fig. 2a that for a fixed
 203 location the σ'_h is at its maximum at $t'=0$ and decreases with time gradually to a
 204 negligible number at $t'=1.0$. This means that the error in $h(x, t)$ predicted by an
 205 analytical or numerical solution due to the uncertain initial condition is significant at

206 early time, especially near a flux boundary. The time duration during which the
 207 effect of the uncertain initial condition is significant depends on the value of the
 208 characteristic timescale (t_c) since $t'=t/t_c$. In the most aquifers this duration may last
 209 many days. In the typical aquifer studied the effect of the uncertainty in initial
 210 condition on $h(x, t)$ is significant during first 250 days ($t'=1.0$). This duration should
 211 be relatively short, however, in a more permeable aquifer whose horizontal extent (L)
 212 is relatively smaller than its thickness (M). It is seen in Fig. 2b that for a fixed time,
 213 the σ'_h is the largest at the left flux boundary ($x'=0.0$) and becomes zero at the right
 214 constant head boundary ($x'=1.0$) since the right boundary is deterministic. This
 215 means that the error in $h(x, t)$ predicted by an analytical or numerical solution due to
 216 the uncertain initial condition is significant almost everywhere in the aquifer: the
 217 further away from a constant head boundary, the larger the error.

218 We then consider the uncertainty in the areal source/sink term (W) by setting
 219 $\sigma_{W_0}^2 = \sigma_Q^2 = \sigma_H^2 = 0$. In this case the dimensionless variance in Eq. (8) reduces to

$$220 \sigma'^2_h(x', t') = 2 \sum_{m=0}^{\infty} \sum_{n=0}^{\infty} \cos(b'_m x') \cos(b'_n x') \frac{(1 - e^{-2b'_m t'})(-1)^{m+n}}{(b'_m^2 + b'_n^2) b'_m b'_n} \quad (12)$$

221 where $\sigma'^2_h = \sigma_h^2 TS_Y / (4L^2 \sigma_W^2 \lambda_W)$. The changes of the σ'_h with x' and t' were
 222 presented in Fig 2c and 2d, respectively. It is noticed in Fig. 2c that at a fixed location,
 223 the σ'_h is zero initially, gradually increases as time goes, and approaches a constant
 224 limit at later time. This means that the error in $h(x, t)$ due to an source/sink is at its
 225 minimum at early time and increases with time to approach a constant limit at later
 226 time: the closer to the left flux boundary, the larger the limit. For a fixed time the
 227 σ'_h decreases smoothly from the left to the right boundary (Fig. 2d). The error in $h(x,$

228 t) due to the uncertainty in the source/sink is significant almost everywhere in the
 229 aquifer: the further away from the constant head boundary, the larger the error, similar
 230 to the previous case with the random initial condition (Fig. 2b).

231 Thirdly, we investigate the effect of the left random flux boundary by setting
 232 $\sigma_{W_0}^2 = \sigma_W^2 = \sigma_H^2 = 0$ in Eq. (8). In this case the dimensionless head variance is given
 233 by

$$234 \quad \sigma_h'^2(x', t') = 2 \sum_{m=0}^{\infty} \sum_{n=0}^{\infty} \cos(b'_m x') \cos(b'_n x') \frac{1 - e^{-2b_m'^2 t'}}{b_m'^2 + b_n'^2} \quad (13)$$

235 where $\sigma_h'^2 = \sigma_h^2 T S_Y / (4 \sigma_Q^2 \lambda_Q)$. The changes of the σ_h' with x' and t' were
 236 presented in Fig 2e and 2f, respectively. At any location the σ_h' in Fig. 2e or the
 237 error in $h(x, t)$ due to an uncertain flux boundary is at its minimum at early time and
 238 increases quickly with time to approach a constant limit: the closer to the left flux
 239 boundary, the larger the limit. At any time the σ_h' in Fig. 2f or the error in the head
 240 due to the uncertain flux boundary is at its maximum at the left boundary but
 241 decreases quickly away from the boundary to become insignificant for $x' > 0.8$.

242 Fourthly, we investigated the effect of the random head boundary by setting
 243 $\sigma_{W_0}^2 = \sigma_W^2 = \sigma_Q^2 = 0$ in Eq. (8). The dimensionless head variance in this case is given
 244 by

$$245 \quad \sigma_h'^2(x', t') = 2 \sum_{m=0}^{\infty} \sum_{n=0}^{\infty} \cos(b'_m x') \cos(b'_n x') \frac{(-1)^{m+n} b'_m b'_n (1 - e^{-2b_m'^2 t'})}{(b_m'^2 + b_n'^2)} \quad (14)$$

246 where $\sigma_h'^2 = \sigma_h^2 L^2 S_Y / (4 T \sigma_H^2 \lambda_H)$. The changes of this σ_h' with x' and t' were
 247 presented in Fig 2g and 2h, respectively. It seen in Fig. 2g that at any location the
 248 σ_h' or the error in $h(x, t)$ due to the random head boundary increases with time

249 quickly to approach a constant limit: the closer to the uncertain head boundary, the
 250 larger the error. The spatial variation of σ'_h can be clearly observed in Fig. 2h for
 251 fixed t' . At any time σ'_h is at its maximum at the right boundary ($x'=1$) where the
 252 head is uncertain, decreases quickly away from the boundary. The error in $h(x, t)$ due
 253 to the uncertain head boundary is limited in a narrow zone near the boundary ($x'>0.8$)
 254 (Fig. 2h).

255 Finally, we consider the combined effects of the uncertainties from all four
 256 sources, i.e., the initial condition, sources, and flux and head boundaries. The head
 257 variance in Eq. (8) is written in the dimensionless form as

$$258 \quad \sigma'^2_h(x', t') = \sum_{m=0}^{\infty} \sum_{n=0}^{\infty} \cos(b'_m x') \cos(b'_n x') \left\{ e^{-(b'_m^2 + b'_n^2)t'} \frac{(-1)^{m+n} \sigma'^2_{W_0}}{b'_m^3 b'_n^3} + \right. \\ \left. 2 \frac{1 - e^{-2b'_m^2 t'}}{(b'_m^2 + b'_n^2)} \left[\frac{(-1)^{m+n}}{b'_m b'_n} + \sigma'^2_Q + (-1)^{m+n} b'_m b'_n \sigma'^2_H \right] \right\} \quad (15)$$

259 where

$$260 \quad \sigma'^2_h = \frac{\sigma_h^2 T S_Y}{4 L^2 \sigma_w^2 \lambda_w}; \quad \sigma'^2_{W_0} = \frac{L^2 S_Y \sigma_{W_0}^2}{T \sigma_w^2 \lambda_w}; \quad \sigma'^2_Q = \frac{\sigma_Q^2 \lambda_Q}{L^2 \sigma_w^2 \lambda_w}; \quad \sigma'^2_H = \frac{T^2 \sigma_H^2 \lambda_H}{L^4 \sigma_w^2 \lambda_w}$$

261 The dimensionless variances, $\sigma'^2_{W_0}$, σ'^2_Q and σ'^2_H , need to be specified in order to
 262 evaluate the dimensionless $\sigma'^2_h(x', t')$ in Eq. (15). For the typical aquifer mentioned
 263 above with $L=100\text{m}$, $T=10 \text{ m}^2/\text{day}$ (or $K=1\text{m/day}$ and $M=10\text{m}$) and $S_Y=0.25$, we
 264 set $\sigma_{W_0}^2 / (\sigma_w^2 \lambda_w) = 10^{-1}$, $\sigma_Q^2 \lambda_Q / (\sigma_w^2 \lambda_w) = 10^3$, $\sigma_H^2 \lambda_H / (\sigma_w^2 \lambda_w) = 10^4$ and obtain
 265 $\sigma'^2_{W_0} = 25$, $\sigma'^2_Q = 0.1$ and $\sigma'^2_H = 0.01$.

266 The changes of this σ'_h with x' and t' were presented in Fig 2i and 2j,
 267 respectively. It is observed in Fig. 2i that at any location the σ'_h is at its maximum

268 due to the uncertainty in the initial condition, gradually decreases as time goes, and
269 approaches a constant limit at later time ($t' > 0.6$) which is due to the combined
270 effects of the uncertain source/sink and flux and head boundaries. This means that
271 the error in the head in early time is significant if the initial condition is uncertain
272 and reduces as time goes to reach a constant limit. The error in head in later time is
273 determined by the uncertainties in the source/sink, flux and head boundaries. It can
274 be observed in Fig. 2j that σ'_{h_i} is relatively larger near both boundaries. The values
275 of σ'_{h_i} at the two boundaries are equivalent (~ 1.3) at early time, say $t' = 0.01$ (the top
276 curve in Fig. 2j) and it reduces slowly away from the flux boundary but quickly
277 away from the head boundary. As time progresses, the σ'_{h_i} near the head boundary
278 stays more or less the same but reduces significantly in most part of the aquifer. This
279 means that in early time the error in $h(x, t)$ in most part of the aquifer is mainly
280 caused by the initial condition and at later time it is due to the combined effects of
281 the uncertain areal source/sink and flux boundary. The effect of the uncertain head
282 boundary on $h(x, t)$ doesn't change with time significantly but is limited in a narrow
283 zone near the boundary.

284 **3.2 Spectrum of groundwater levels**

285 We first evaluated S_{hh} in Eq. (10) due to the effect of the white noise flux
286 boundary only by setting $S_{QQ} \neq 0$, $S_{WW} = 0$, and $S_{HH} = 0$. The dimensionless
287 spectrum S_{hh}/S_{QQ} as a function of the frequency (f) was evaluated and presented in
288 the log-log plot (Fig. 3a-3c) for three values of t_c (40, 400, and 4,000 days) since the
289 value of t_c is 250 days for a sandy aquifer as we mentioned above and at the six

290 locations ($x' = 0.0, 0.2, 0.4, 0.6, 0.8$, and 0.9). The spectrum S_{hh}/S_{QQ} in Fig. 3a is
 291 more or less horizontal (i.e., white noise) at low frequencies and decrease gradually
 292 as f increases, indicating that an aquifer acts as a low-bass filter that filter signals at
 293 high frequencies and keep signals at low frequencies. The aquifer has significantly
 294 dampened the fluctuations of the groundwater level. The spectrum varies with the
 295 location x' : the smaller the value of x' or the closer to the left flux boundary ($x'=0$),
 296 the larger the spectrum (Fig. 3a-3c). All spectra in Fig. 3a are not a straight line in
 297 the log-log plot, meaning that the temporal scaling of $h(x, t)$ doesn't exist in the
 298 range of $f = 10^{-3} \sim 10^0$ when $t_c=40$ days. As t_c increases to 400 and 4000 days,
 299 however, the spectrum at $x'=0$ become a straight line (the top curve in Fig. 3b and 3c)
 300 or has a power-law relation with f , i.e., $S_{hh}/S_{QQ} \propto 1/f$, since its slope is approximately
 301 one. The fluctuations of $h(0, t)$ is a pink noise due to the white noise fluctuations flux
 302 boundary when the characteristic timescale (t_c) is large which means that the aquifer
 303 is relatively less permeable and/or has a much larger horizontal length than its
 304 thickness.

305 Secondly, the spectrum S_{hh}/S_{HH} due to the sole effect of the random head
 306 boundary was evaluated by setting $S_{HH} \neq 0$, $S_{WW} = 0$, and $S_{QQ} = 0$ in Eq. (10) for
 307 the same three values of t_c and six locations and presented in Fig. 3d-3f as a function
 308 of f . It is shown that similar to Fig. 3a-3c, the spectrum decreases as f increases but
 309 different from Fig. 3a-3c, the spectrum is larger at $x'=0.9$ near the right boundary
 310 (the top curves in Fig. 3d-3f) than that $x'=0.0$ (the bottom curves). Furthermore,
 311 none of the spectra are a straight line in the log-log plot, indicating that the temporal

312 scaling of groundwater level fluctuations doesn't exist in the case of the white noise
313 head boundary.

314 Thirdly, the spectrum S_{hh}/S_{WW} due the effect of the white noise recharge only
315 was evaluated by setting $S_{WW} \neq 0$, $S_{QQ} = 0$, and $S_{HH} = 0$ in Eq. (10) for the same
316 values of t_c and x' and presented in Fig. 3g-3i as a function of f . It is shown that
317 when $t_c=40$ day the spectrum in Fig. 3g is horizontal at low frequencies and become
318 a straight line at high frequencies: the closer to the right head boundary, the later it
319 approaches a straight line (Fig. 3h). As t_c increases to 400 and 4000 days, the slope
320 of the spectrum at all locations except at $x'=0.9$ approaches to a straight line with a
321 slope of 2 (Fig. 3h and 3i), indicating a temporal scaling of $h(x, t)$. The fluctuations
322 of groundwater level is a Brownian motion, i.e., $S \propto 1/f^2$, when $t_c \geq 4000$ day or in
323 a relatively less permeable and/or has a much larger horizontal length than its
324 thickness.

325 Finally, the head spectrum due to the combined effect of all three random
326 sources (the white noise recharge, and flux and head boundaries) was evaluated, i.e.,
327 $S_{WW} \neq 0$, $S_{QQ} \neq 0$, and $S_{HH} \neq 0$ in Eq. (10). The spectrum of S_{hh}/S_{WW} as a
328 function of f was presented in Fig. 3j-3l for the same values of t_c and x' where
329 $S_{QQ}/S_{WW} = 1000$ and $S_{HH}/S_{WW} = 10000$ which are same with the values using in
330 previous section. It is noticed that the general patterns of S_{hh}/S_{WW} in the
331 combined case is similar to the case under the random source/sink only (Fig. 3g-3i)
332 except at $x'=0.0$ and 0.9 (the dashed and dotted curves in Fig. 3j, respectively) due
333 to the strong effects of the boundary conditions at these two locations. At $t_c=4000$

334 day, the spectra at all locations except $x'=0.0$ (Fig. 3l) are similar to those in Fig. 3i,
335 indicating the dominating effect of the random areal source/sink. The spectrum at
336 $x'=0$ in this case is also a straight line (the dashed curve in Fig. 3l) but with a
337 different slope due to the effect of the random flux boundary which is similar to the
338 top straight line in Fig. 3c. Above results provide a theoretical explanation as why
339 temporal scaling exists in the observed groundwater level fluctuations (Zhang and
340 Schilling, 2004; Bloomfield and Little, 2010; Zhu et al., 2012). We thus conclude that
341 temporal scaling of $h(x, t)$ may indeed exist in real aquifers due to the strong effect
342 of the areal source/sink.

343 **4. Conclusions**

344 In this study the effects of random source/sink, and initial and boundary
345 conditions on the uncertainty and temporal scaling of the groundwater level, $h(x, t)$
346 were investigated. The analytical solutions for the variance, covariance and spectrum
347 of $h(x, t)$ in an unconfined aquifer described by a linearized Boussinesq equation
348 with white noise source/sink, and initial and boundary conditions were derived. The
349 standard deviations of $h(x, t)$ for various cases were evaluated. Based on the results,
350 the following conclusions can be drawn.

351 1. The error in $h(x, t)$ due to a random initial condition is significant at early
352 time, especially near a flux boundary. The duration during which the effect is
353 significant may last a few hundred days in most aquifers;

354 2. The error in $h(x, t)$ due to a random areal source/sink is significant in most
355 part of an aquifer: the closer to a flux boundary, the larger the error;

356 3. The errors in $h(x, t)$ due to random flux and head boundaries are significant
357 near the boundaries: the closer to the boundaries, the larger the errors. The random
358 flux boundary may affect the head over a larger region near the boundary than the
359 random head boundary;

360 4. In the typical sandy aquifer studied (with the length of aquifer at the
361 direction of water flow $L=100\text{m}$, the average saturated thickness $M=10\text{m}$, hydraulic
362 conductivity $K=1\text{m/day}$, and specific yield $S_Y=0.25$) the error in $h(x, t)$ in early time
363 is mainly caused by an uncertain initial condition and the error reduces as time goes
364 to reach a constant error in later time. The constant error in $h(x, t)$ is mainly due to
365 the combined effects of uncertain source/sink and boundaries;

366 5. The aquifer system behaves as a low-pass filter which filter the short-term
367 (high frequencies) fluctuations and keep the long-term (low frequencies)
368 fluctuations;

369 6. Temporal scaling of groundwater level fluctuations may indeed exist in
370 most part of a low permeable aquifer whose horizontal length is much larger than its
371 thickness caused by the temporal fluctuations of areal source/sink.

372 Finally, it is pointed out that the analyses carried out in this study is under the
373 assumptions that the processes, $W(t)$, $Q(t)$, and $H(t)$ are uncorrelated white noises. In
374 reality, they may be correlated and spatially varied. We plan to relax those constraints
375 and study more realistic cases in the near future. It is also noted that the analytical
376 solutions for head variances derived in this study provide a way to identify and
377 quantify the uncertainty. The spectrum relationship obtained among the head,

378 recharge and boundary conditions can help one to improve spectrum analysis for a
379 groundwater level time series and removed the effects of the boundary conditions.

380 **Acknowledgment**

381 This study was partially supported with the research grants from the National
382 Nature Science Foundation of China (NSFC-41272260; NSFC-41330314;
383 NSFC-41302180), the Natural Science Foundation of Jiangsu Province
384 (SBK201341336) and from the National Key project “Water Pollution Control in the
385 Huai River Basin” of China (2012ZX07204-001, 2012ZX07204-003).

386 **References**

387 Bear, J.: Dynamics of fluids in porous media, Environmental science series (New York, 1972-),
388 American Elsevier Pub. Co., New York, xvii, 764 p. pp., 1972.

389 Beven, K., and Binley, A.: The Future of Distributed Models - Model Calibration and Uncertainty
390 Prediction, Hydrol Process, 6, 279-298, 1992.

391 Bloomfield, J. P., and Little, M. A.: Robust evidence for random fractal scaling of groundwater levels
392 in unconfined aquifers, J Hydrol, 393, 362-369, DOI 10.1016/j.jhydrol.2010.08.031, 2010.

393 Dagan, G.: Flow and transport in porous formations, Springer-Verlag, Berlin ; New York, xvii, 465 p.
394 pp., 1989.

395 Gelhar, L. W.: Stochastic subsurface hydrology, Prentice-Hall, Englewood Cliffs, N.J., x, 390 p. pp.,
396 1993.

397 Hantush, M. M., and Marino, M. A.: One-Dimensional Stochastic-Analysis in Leaky Aquifers Subject
398 to Random Leakage, Water Resour Res, 30, 549-558, Doi 10.1029/93wr02887, 1994.

399 Liang, X. Y., and Zhang, Y. K.: A new analytical method for groundwater recharge and discharge
400 estimation, J Hydrol, 450, 17-24, DOI 10.1016/j.jhydrol.2012.05.036, 2012.

401 Liang, X. Y., and Zhang, Y. K.: Temporal and spatial variation and scaling of groundwater levels in a
402 bounded unconfined aquifer, J Hydrol, 479, 139-145, DOI 10.1016/j.jhydrol.2012.11.044,
403 2013a.

404 Liang, X. Y., and Zhang, Y. K.: Analytic solutions to transient groundwater flow under
405 time-dependent sources in a heterogeneous aquifer bounded by fluctuating river stage, Adv
406 Water Resour, 58, 1-9, DOI 10.1016/j.advwatres.2013.03.010, 2013b.

407 Neuman, S. P.: Maximum likelihood Bayesian averaging of uncertain model predictions, Stoch Env
408 Res Risk A, 17, 291-305, 10.1007/s00477-003-0151-7, 2003.

409 Neuman, S. P., Xue, L., Ye, M., and Lu, D.: Bayesian analysis of data-worth considering model and
410 parameter uncertainties, Advances in Water Resources, 36, 75-85,
411 10.1016/j.advwatres.2011.02.007, 2012.

412 Nowak, W., de Barros, F. P. J., and Rubin, Y.: Bayesian geostatistical design: Task-driven optimal site
413 investigation when the geostatistical model is uncertain, *Water Resour Res*, 46, Artn W03535
414 Doi 10.1029/2009wr008312, 2010.

415 Priestley, M. B.: *Spectral Analysis and Time Series*, Academic Press, San Diego, 1981.

416 Refsgaard, J. C., van der Sluijs, J. P., Hojberg, A. L., and Vanrolleghem, P. A.: Uncertainty in the
417 environmental modelling process - A framework and guidance, *Environmental Modelling &*
418 *Software*, 22, 1543-1556, 10.1016/j.envsoft.2007.02.004, 2007.

419 Rojas, R., Feyen, L., and Dassargues, A.: Conceptual model uncertainty in groundwater modeling:
420 Combining generalized likelihood uncertainty estimation and Bayesian model averaging, *Water
421 Resources Research*, 44, 10.1029/2008wr006908, 2008.

422 Rojas, R., Feyen, L., Batelaan, O., and Dassargues, A.: On the value of conditioning data to reduce
423 conceptual model uncertainty in groundwater modeling, *Water Resources Research*, 46, 20,
424 10.1029/2009wr008822, 2010.

425 Schilling, K. E., and Zhang, Y. K.: Temporal Scaling of Groundwater Level Fluctuations Near a
426 Stream, *Ground Water*, 50, 59-67, DOI 10.1111/j.1745-6584.2011.00804.x, 2012.

427 Vrugt, J. A., Gupta, H. V., Bouten, W., and Sorooshian, S.: A Shuffled Complex Evolution Metropolis
428 algorithm for optimization and uncertainty assessment of hydrologic model parameters, *Water
429 Resources Research*, 39, 10.1029/2002wr001642, 2003.

430 Ye, M., Meyer, P. D., and Neuman, S. P.: On model selection criteria in multimodel analysis, *Water
431 Resources Research*, 44, 10.1029/2008wr006803, 2008.

432 Zeng, X. K., Wang, D., Wu, J. C., and Chen, X.: Reliability Analysis of the Groundwater Conceptual
433 Model, *Human and Ecological Risk Assessment*, 19, 515-525, 10.1080/10807039.2012.713822,
434 2013.

435 Zhang, D.: *Stochastic methods for flow in porous media : coping with uncertainties*, Academic, San
436 Diego, Calif. London, xiv, 350 p. pp., 2002.

437 Zhang, Y. K., and Schilling, K.: Temporal scaling of hydraulic head and river base flow and its
438 implication for groundwater recharge, *Water Resour Res*, 40, -, Artn W03504
439 Doi 10.1029/2003wr002094, 2004.

440 Zhang, Y. K., and Li, Z. W.: Temporal scaling of hydraulic head fluctuations: Nonstationary spectral
441 analyses and numerical simulations, *Water Resources Research*, 41, 10.1029/2004wr003797,
442 2005.

443 Zhang, Y. K., and Li, Z. W.: Effect of temporally correlated recharge on fluctuations of groundwater
444 levels, *Water Resources Research*, 42, 10.1029/2005wr004828, 2006.

445 Zhang, Y. K., and Yang, X. Y.: Effects of variations of river stage and hydraulic conductivity on
446 temporal scaling of groundwater levels: numerical simulations, *Stoch Env Res Risk A*, 24,
447 1043-1052, DOI 10.1007/s00477-010-0437-5, 2010.

448 Zhu, J. T., Young, M. H., and Osterberg, J.: Impacts of riparian zone plant water use on temporal
449 scaling of groundwater systems, *Hydrol Process*, 26, 1352-1360, Doi 10.1002/Hyp.8241, 2012.

450

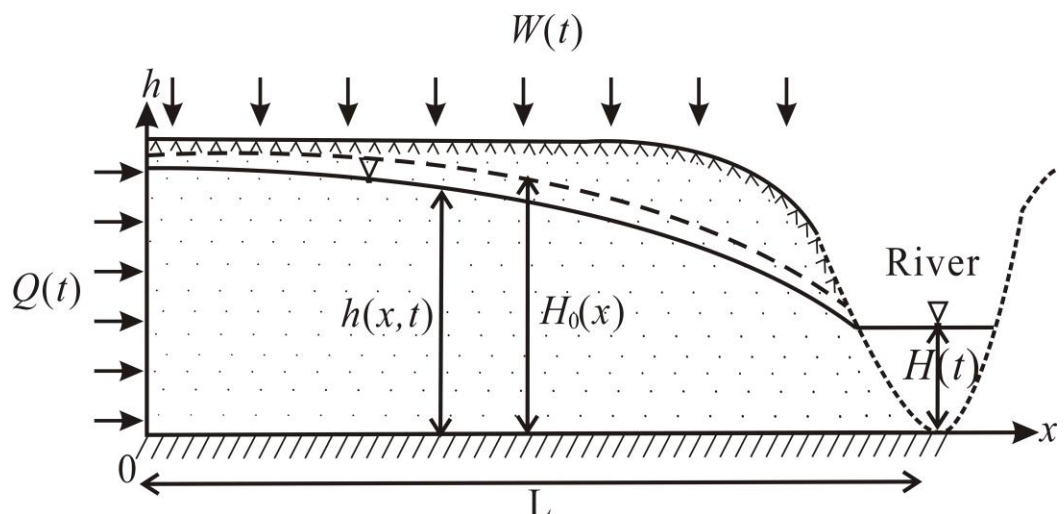
451

Figure captions

Figure 1 A schematic of the unconfined aquifer studied where $W(t)$ is the random time-dependent source/sink, $H_0(x)$ is the random initial condition, $Q(t)$ is the random time-dependent flux at the left boundary, $H(t)$ is the random time-dependent water level at the right boundary, L is distance from the left to the right boundary, and $h(x, t)$ is the random groundwater level in the aquifer.

Figure 2 The graphs on the left column are the standard deviation (σ'_h) of groundwater level ($h(x, t)$) versus the dimensionless time (t') at the dimensionless locations $x'=0.0, 0.2, 0.4, 0.6$, and 0.8 . The graphs on the right column are σ'_h versus x' for the different t' : b) and d) are for $t'=0.0, 0.2, 0.4, 0.6$ and 0.8 , f) and h) are for $t'=0.01, 0.1$, and 1.0 , and j) is for $t'=0.01, 0.2, 0.4, 0.6$ and 0.8 . Also, a) and b) are based on Eq.(11) where $\sigma_w^2 = \sigma_Q^2 = \sigma_H^2 = 0$; c) and d) are based on Eq. (12) where $\sigma_{W_0}^2 = \sigma_Q^2 = \sigma_H^2 = 0$; e) and f) are based on Eq. (13) where $\sigma_{W_0}^2 = \sigma_w^2 = \sigma_H^2 = 0$; g) and h) are based on Eq. (14) where $\sigma_{W_0}^2 = \sigma_w^2 = \sigma_Q^2 = 0$; i) and j) are based on Eq.(15) where $\sigma_{W_0}^2 \neq \sigma_w^2 \neq \sigma_Q^2 \neq \sigma_H^2 \neq 0$.

Figure 3 The dimensionless power spectrum versus frequency (f) at the dimensionless locations $x'=0.0, 0.2, 0.4, 0.6, 0.8$, and 0.9 . The graphs on the left column are for $t_c = 40$ day, the graphs on the middle column are for $t_c = 400$ day, and the graphs on the right column are for $t_c = 4000$ day. The graphs on the first row are the dimensionless spectrum S_{hh}/S_{QQ} when $S_{ww}=0$, $S_{HH}=0$, and $S_{QQ} \neq 0$ in Eq. (10), the graphs on the second row is S_{hh}/S_{HH} when $S_{ww}=0$, $S_{QQ}=0$, and $S_{HH} \neq 0$, the graphs on the third row are S_{hh}/S_{ww} when $S_{QQ}=0$, $S_{HH}=0$, and $S_{ww} \neq 0$, and the graphs on the bottom row is S_{hh}/S_{WW} when $S_{QQ} \neq 0$, $S_{HH} \neq 0$, and $S_{WW} \neq 0$.



479

480

481

482

Figure 1

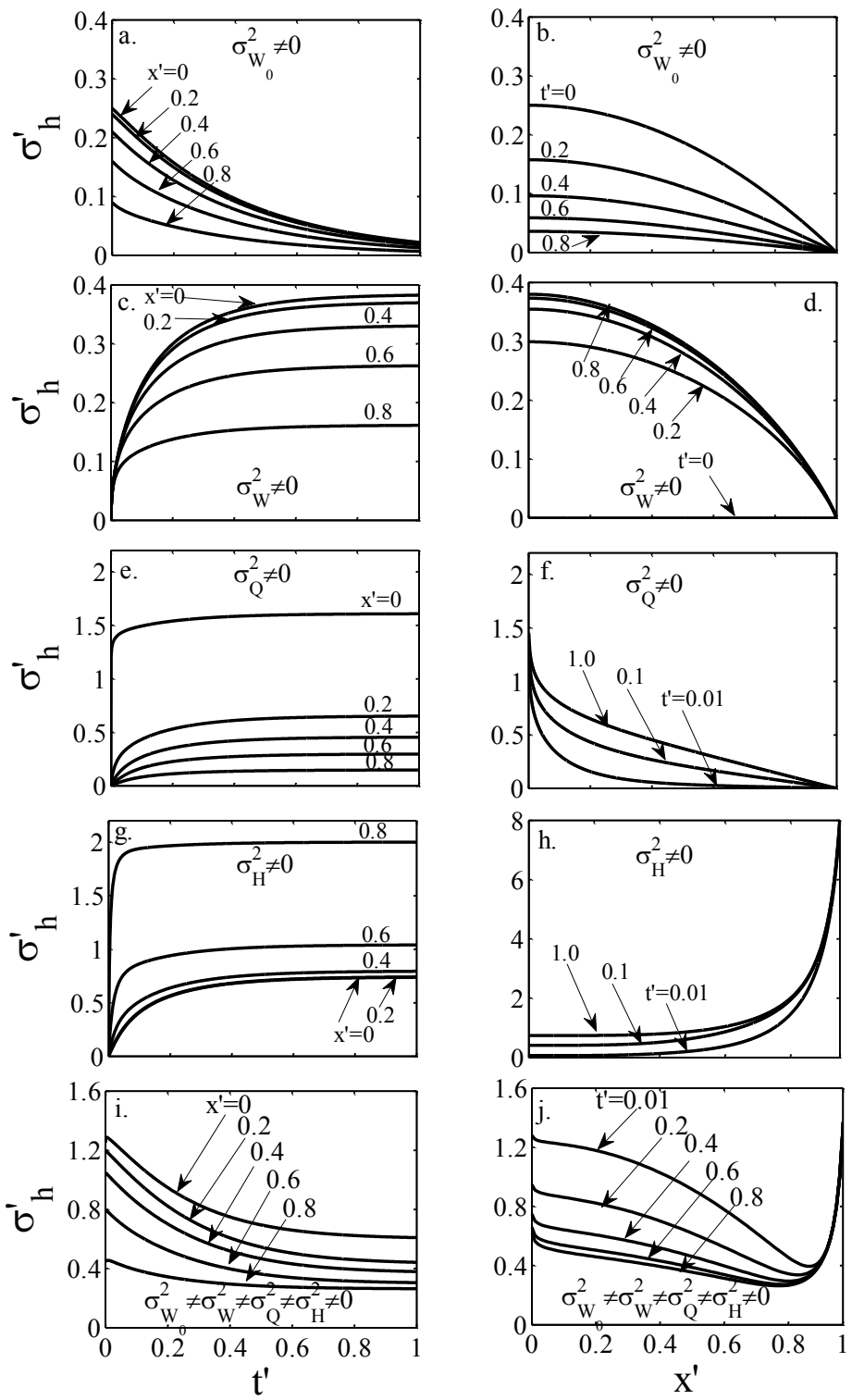


Figure 2

483

484

485

486

